Chikungunya virus fusion properties elucidated by single-particle and bulk approaches

van Duijl-Richter, Mareike K. S.; Blijleven, Jelle S.; van Oijen, Antoine M.; Smit, Jolanda M.

Published in:
The Journal of general virology

DOI:
10.1099/vir.0.000144

Publication date:
2015

Chikungunya virus fusion properties elucidated by single-particle and bulk approaches

Author names: Mareike K. S. van Duijl-Richter [1¤], Jelle S. Blijleven [2¤], Antoine M. van Oijen [2,3#], Jolanda M. Smit [1#]

¤,# These authors contributed equally to this work.

Author affiliations:

[1]: Department of Medical Microbiology, University Medical Center Groningen, University of Groningen, 9700 RB Groningen, The Netherlands

[2]: Centre for Synthetic Biology, Zernike Institute of Advanced Materials, University of Groningen, 9747 AG Groningen, the Netherlands

[3]: School of Chemistry, University of Wollongong, Wollongong, NSW 2522, Australia

 # Corresponding authors:

Jolanda Smit, E: jolanda.smit@umcg.nl, T: +31 50 3632738

Antoine van Oijen, E: vanoijen@uow.edu.au, T: +61 (0)2 4221 4780

Abstract

Chikungunya virus (CHIKV) is a rapidly spreading, enveloped alphavirus causing fever, rash and debilitating polyarthritis. No specific treatment or vaccines are available to treat or prevent infection. For the rational design of vaccines and antiviral drugs, it is imperative to understand the molecular mechanisms involved in CHIKV infection. A critical step in the life cycle of CHIKV is fusion of the viral membrane with a host cell membrane. Here, we elucidate this process using ensemble-averaging liposome-virus fusion studies, in which the fusion behavior of a large virus population is measured, and a newly developed microscopy-based single-particle assay, in which the fusion kinetics of an individual particle can be visualized. The combination of these approaches allowed us to obtain detailed insight in the kinetics, lipid dependency, and pH dependency of hemifusion. We found that CHIKV fusion is strictly dependent on low pH, with a threshold of pH 6.2 and optimal fusion efficiency below pH 5.6. At this pH, CHIKV fuses rapidly with target membranes, with typically half of the fusion occurring within less than two seconds after acidification. Cholesterol and sphingomyelin in the target membrane were found to strongly enhance the fusion process. By analysing our single-particle data using kinetic models, we were able to derive that the number of rate-limiting steps occurring before hemifusion equals about three. To explain these data, we propose a mechanistic model in which multiple E1 fusion trimers are involved in initiating the fusion process.

Introduction

Chikungunya virus (CHIKV) is a rapidly emerging pathogen that belongs to the alphavirus genus, which also includes Semliki Forest virus (SFV), Sindbis virus (SINV) and O'nyong O'nyong virus (ONNV) (Leung *et al*., 2011; Powers *et al*., 2001). After re-emerging in 2004, CHIKV has caused large epidemics in Africa and Asia (Enserink, 2007; Schwartz & Albert, 2010) and a number of cases in Europe (Tomasello & Schlagenhauf, 2013). Recently, CHIKV crossed the Atlantic (Enserink, 2014; Fischer *et al*., 2014) and as of January 2015, more than 26,000 confirmed and 1,094,000 suspected CHIKV cases were reported in the Americas (Centers for Disease Control and Prevention, 2015).

CHIKV is transmitted by *Aedes* mosquitos, with *A. aegypti* and *A. albopictus* as the most important vectors (Sourisseau *et al*., 2007; Tsetsarkin *et al*., 2007). The majority of people infected with CHIKV develop chikungunya fever, which is characterized by high fever, rash, myalgia, joint pain, and headache. A common long-term implication of CHIKV fever is severe joint pain, which can persist for months to years. There is no vaccine or specific treatment for CHIKV available (Burt *et al*., 2012; Kucharz & Cebula-Byrska, 2012; Sourisseau *et al*., 2007; Thiberville *et al*., 2013). For the rational design of a vaccine or antiviral drug it is imperative to acquire detailed knowledge on the molecular mechanisms involved in CHIKV infection.

Alphaviruses are enveloped viruses that infect the cell via receptor-mediated endocytosis and subsequent membrane fusion from within acidic endosomes (Kielian *et al*., 2010; Strauss & Strauss, 1994), although direct fusion at the plasma membrane has also been reported (Vancini *et al*., 2013). Viral attachment and fusion are facilitated by the envelope glycoproteins E1 and E2, which are arranged as 80 spikes at the viral surface (Lescar *et al*., 2001). One spike consists of three E1/E2 heterodimers. The E2 protein contains the receptor-binding site and shields the fusion loop on E1 (Li *et al*., 2010; Voss *et al*., 2010). Upon virus uptake and delivery to endosomes, the acidic pH of the endosomal lumen causes a dramatic rearrangement within the E1/E2 heterodimers, which drives fusion of the viral membrane with the endosomal membrane. The first step in this process involves dissociation of the E1/E2 heterodimer (Wahlberg *et al*., 1989, Wahlberg & Garoff, 1992). As a consequence, the fusion loop is exposed and inserted into the target host membrane (Gibbons *et al*., 2004a). A core trimer of E1 proteins is formed and the E1 subunits re-fold, which causes the opposing proximal membrane leaflets to merge, a step known as hemifusion (Sanchez-San Martin *et al*., 2008). Subsequently, a fusion pore is formed and the viral nucleocapsid is released into the cytosol (Wengler *et al*., 2004). Generally, multiple copies of a viral protein trimer are thought to act in concert to catalyse hemifusion (Harrison, 2008).

The characteristics of the membrane fusion reaction have been studied in detail for the alphaviruses SFV and SINV (reviewed in Kielian *et al*., 2010). For both viruses, membrane fusion is strictly dependent on low pH and the presence of sphingomyelin and cholesterol in the host cell membrane (Lu *et al*., 1999; Nieva *et al*., 1994; Smit *et al*., 1999; White & Helenius, 1980). Fusion is not dependent on the presence of a protein receptor in the target membrane. In liposomal bulk fusion assays, the threshold of fusion has been found to be pH 6.2 for SFV and 6.0 for SINV wild-type strains (Bron *et al*., 1993; Smit *et al*., 1999). However, this threshold varies with strain and assessment method, as also lower pH thresholds for both viruses were described (Glomb-Reinmund & Kielian, 1998). For CHIKV, cell-based assays revealed that fusion is dependent on low pH and cholesterol as well (Bernard *et al*., 2010; Gay *et al*., 2012). The pH threshold of fusion is around pH 5.9-6.1, depending on the strain

used (Sanchez-San Martin *et al*., 2013; Tsetsarkin *et al*., 2011). However, no details are known on the membrane fusion kinetics or sphingomyelin dependence of fusion.

In this study, we characterized the kinetics of CHIKV (strain S27) fusion using both a liposomal bulk fusion assay and a single-particle fusion assay based on total-internal-reflection fluorescence microscopy (TIRF-M). We found that CHIKV fusion is strictly dependent on low pH, with a pH threshold of 6.2 and optimal fusion at a pH range of 4.5-5.6. For this CHIKV strain, we observed a sharp pH dependency of the extent of fusion, with only 0.3 pH units between conditions of near-maximal and only residual fusion activity. Both cholesterol and sphingomyelin in the host-cell membrane strongly supported CHIKV fusion activity. The single-particle assay indicated that multiple, parallel rate-limiting steps precede hemifusion, a phenomenon described earlier for other membrane-fusing viruses (Brandenberg *et al*., 2015; Costello *et al*., 2012; Danieli *et al*., 1996; Floyd *et al*., 2008). We propose that these steps are arising from the parallel action of several fusion trimers.

Results

pH-dependent fusion of CHIKV with liposomes. For the bulk fusion assay, CHIKV was biosynthetically labelled with 1-pyrenehexadecanoic acid (pyrene) (Pal *et al*., 1988). The pyrene labelling did not influence viral infectivity (shown in Table S1). The virus was incubated with liposomes and fusion was triggered by adding a pre-titrated volume of low-pH buffer to the reaction mixture. Fusion was followed in real time using a fluorimeter at 37°C. The lipid concentration corresponding to optimal fusion efficiency and signal-to-noise ratio was determined to be 400 μM, and therefore used for all experiments (Fig. S1).

Fig. 1(a) shows the time traces of the extent of CHIKV fusion at different pH values as measured by the bulk assay (solid lines). The total extent of fusion as a function of pH is shown in Fig. 1(b). The highest pH showing detectable fusion was pH 6.2, with a residual fusion activity of 4.3±0.6%, compared to the pH 7.4 control (0±2%). For the CHIKV S27 strain used, we observed a sharp pH dependence: a change of 0.2 units from pH 5.9 to 6.1 resulted in an eight-fold reduction of the extent of fusion, suggesting a fusion mechanism that involves a form of cooperativity between neighboring fusion proteins. Below pH 5.6, the extent of fusion reaches a plateau value. The fusion rate, which we calculated as the inverse of the time point at which half of the extent of fusion is reached, is plotted in Fig. 1(c). In the bulk assay, the fusion rate was observed to increase with lower pH from a minimal, detection-limited value at pH 6.0-6.2, to saturating rate at pH 5.6. In the plateau region, CHIKV fusion happened promptly, with typically half of the fusion occurring within less than two seconds after acidification. The mid points of fusion extent and fusion rate were found to be 0.2 pH units apart.

Earlier work on SFV and SINV showed that the time to induce fusion is very limited, as the E1 protein rapidly rearranges into a fusion-inactive state if acidification occurs in the absence of target membranes (Smit *et al*., 1999; Waarts *et al*., 2005). To assess whether this also applies to CHIKV, virions were exposed to low pH in the absence of liposomes. At the indicated time points in Fig. 2(a), pre-acidified liposomes were added to the acidic virus-containing reaction mixture. A tenfold reduction in fusion extent was observed in 9±2 s. This inactivation curve is faster than for SFV (~50 seconds for a tenfold reduction) and for SINV (~75 seconds). The inactivation was not described well by a single inactivation rate, but instead a sum of two exponentials was required to describe the data (Fig. 2a; dotted curve). The fast-decaying fraction represented 76±5% of the total population, decaying at a time scale of τ = 4.2±0.4 s. The remaining 24±5% inactivated with a time constant of τ = 38±5 s. To test whether inactivation was reversible, virus was acidified in the absence of liposomes for 90 s at pH 5.0, back-neutralised to pH 8, and a standard fusion measurement was performed. Inactivation was found to be partially reversible (Fig. 2b). Approximately 55% of membrane fusion capacity was restored, when compared to the untreated control that was acidified after the same time interval (Fig. 2c). This is slightly more than the one found for SFV (45%) (Waarts *et al.*, 2005).

Low-pH dependent fusion of single CHIKV particles at 37 °C. The time traces of fusion obtained in the bulk assay represent an averaged readout of an ensemble of virions in different stages of the fusion process. Due to the stochastic nature of the underlying molecular transition, the population becomes increasingly asynchronized as time elapses after triggering fusion. As a result, subpopulations and short-lived intermediate states cannot be discriminated. To overcome this population averaging and obtain more kinetic detail, we designed a single-particle assay based on earlier single-particle work by our group (Floyd *et al*., 2008) and others (Hinterdorfer *et al*., 1994; Imai *et al*., 2006; Ivanovic *et al*., 2013; Melikyan *et al*., 2005; Niles & Cohen.,

1991; Wessels *et al*., 2007) (Fig. 3). We modified our earlier experimental design (Floyd *et al*., 2008) to enable the observation of fusion both at elevated temperatures and with short acidification times (see also Materials and Methods). Purified CHIKV particles were labelled with octadecyl rhodamine B (R18) as described before (Hoekstra *et al*., 1984). R18 labelling did not influence the specific infectivity of the virus (Table S1). After introduction of the labelled virus to the surface-supported lipid bilayer in the flow cell, we observed that the particles bind to the membrane in a nonspecific manner, likely mediated by electrostatic interactions (Fig. 3c; red channel in left panel). Fusion was triggered by a rapid injection of low-pH buffer from a proximal storage channel in the microfluidic flow cell. Hemifusion of individual virions was visualized using TIRF microscopy (Fig. 3a). The flow cell was kept constant at 37±1 °C and acidification of the channel was achieved within 0.9 s. On a particle-by-particle basis, R18 dequenching traces were extracted from the fluorescence movies (Fig. 3c) and the elapsed time between acidification and hemifusion was determined.

Representative curves showing the percentage of particles in the field of view that fused over time are shown in Fig. 1(a) (dashed lines), revealing similar population-level kinetics as in the bulk assay. Mean extents of fusion at t=60 s are plotted in Fig. 1(b) (open squares). The population-level fusion rate, calculated here as the inverse of the median fusion time, is plotted in Fig. 1(c) (open squares). As depicted in the graph, the main features of CHIKV pH-dependent fusion found in the bulk assay were reproduced in the single-particle assay.

Efficient CHIKV fusion is dependent on cholesterol and sphingomyelin in the target membrane. Following previous observations that SINV and SFV fusion is dependent on cholesterol and sphingomyelin in the target membrane (Lu *et al*., 1999; Nieva *et al*., 1994; Smit *et al*., 1999; White & Helenius., 1980), we investigated the fusion characteristics of CHIKV with membranes consisting of varying concentrations of these lipids. As expected, cholesterol in the target membrane strongly supported CHIKV fusion (Fig. 4a; top and middle panels). The total fusion extent followed a sigmoidal curve, with higher amounts of cholesterol in the target membrane leading to higher extents of fusion. Maximal fusion was found at 38-42 mol-% of cholesterol in the target membrane. The fusion rate did not differ considerably between the different cholesterol concentrations (Fig. 4a; bottom panel).

Furthermore, membrane fusion was strongly enhanced by sphingomyelin in the target membrane (Fig. 4b top and middle panels). In contrast to the sigmoidal cholesterol dependency, relatively low amounts of sphingomyelin were sufficient to achieve optimal fusion. The total extent of fusion using membranes containing 22.2 mol-%, 11.1 mol-% and 6.6 mol-% was equal to the maximum observed. Even if the sphingomyelin concentration was reduced 10-fold compared to the standard liposome composition (from 22% to 2.2%), still about 27% of the particles fused with liposomes. Also here, the fusion rate did not vary significantly with target membrane sphingomyelin content (Fig. 4b; bottom panel).

Hemifusion of CHIKV is a process with multiple rate-limiting steps. The data described above demonstrate that the bulk and single-particle fusion assays are mutually consistent in the quantitative information they provide on the extent of fusion and its kinetics at the population level. The strength of the single-particle approach lies in the fact that a particle-by-particle analysis of the kinetics provides additional information which is not accessible by the bulk approach. To evaluate the kinetic determinants for CHIKV fusion, the time elapsed between pH drop and hemifusion was obtained for a large number of particles for two pH points close to the threshold of fusion (pH 6.2 and 6.0) and one pH point within the optimum pH of fusion (pH 4.7).

The distributions of virion lag times from the time of acidification to the hemifusion event are shown in Fig. 5. At all three pH points, the frequency distributions show a rise and decay. We analysed these distributions by fitting them to gamma functions that provide a fitting parameter N describing the number of rate-limiting steps occurring before hemifusion. We showed previously (Floyd et al., 2010) that this is a powerful tool to determine the number of kinetic intermediates in a process. A single rate-limiting step results in a single-exponential distribution and multiple rate-limiting steps introduce the rise-and-decay in the histogram. Performing the fits with gamma functions resulted in $N = 2.1 \pm 0.4$ for pH 6.2 and $N = 3.2 \pm 0.4$ for pH 6.0. At pH 4.7, the typical timescale of hemifusion and the time to drop the pH become comparable in magnitude. To make sure the observed rise-and-decay cannot be explained solely from the pH drop, we did a correction in the fit (see Supplementary information, Fig. S2). Taking the effect of the finite width of the pH drop into account, we obtained a value of $N = 3$ for pH 4.7 (Fig. 5 and Supplementary Fig. S3).

Discussion

Fusion of CHIKV with endosomal membranes is a crucial process in the viral life cycle that has not yet been investigated in great detail. In our study, we established two assays to measure CHIKV fusion *in vitro* at 37°C with remarkable agreement between these approaches. We observed that CHIKV fusion is receptor-independent, triggered by low pH, and enhanced by cholesterol and sphingomyelin in the target membrane. With this approach, we were able to obtain detailed kinetic information on the fusion process up to and including hemifusion.

We observed fusion of the majority of the viral particles within seconds after acidification. This observation is in line with earlier results on the other alphaviruses SINV and SFV (Smit *et al*., 1999; Waarts *et al*., 2005). A slightly higher rate is observed in the single-particle assay (Fig. 1c). This may be explained by the fact that in the single-particle experiments all observed particles are already docked to the membrane before lowering of the pH, while in the bulk assay a subpopulation of virions may still have to associate with a liposome after acidification.

We found that the fusion threshold for CHIKV is pH 6.2. Optimal fusion occurs within the pH range of 4.5-5.6. Remarkably, the pH dependence of fusion for the S27 strain is very sharp: there is an eightfold reduction of fusion extent over 0.2 pH units. This pattern suggests that there is a high degree of cooperativity involved in the steps leading to hemifusion (Kielian, 2014). A similarly sharp pH dependence was observed for the fusion rate, although with its half-point shifted 0.2 pH units towards lower pH. This is most visible at pH 6 and might be due to bound particle pre-selection. The steepness of the pH dependence seems to be related at least partially to the amino acid at the E1 226 position. We and others (Tsetsarkin *et al*., 2011; unpublished results) observed that CHIKV strains with an alanine at this position (like S27) exhibit a sharper pH dependence than strains with a valine at E1 226. Together with the altered cholesterol dependence observed in strains with an A226V mutation, this change might have an influence on the location of viral fusion within the endosomal pathway and subsequently alter viral fitness (Tsetsarkin *et al*., 2007; Tsetsarkin *et al*., 2011).

Pre-exposing CHIKV to low pH for different time intervals showed a reduction in extent of fusion of tenfold over 9±2 s, corresponding to an inactivation rate of k_{inact} = 0.24±0.04 s^{-1}, which is of similar magnitude as the overall fusion rate observed in both assays. We speculate that there is a competition between activation and inactivation of fusogenic trimers at the viral surface under low pH conditions. Within a limited time window, a minimal number of trimers need to act simultaneously to mediate fusion before inactivation occurs. Residual fusion activity remained at high time intervals, suggesting heterogeneity in this CHIKV strain. We modelled this with a double-exponential model, and found a fast-fusing and quickly inactivating population (~76%) and a second population having longer fusion times and slowly inactivating (~24%).

CHIKV fusion is strongly enhanced by the presence of both cholesterol and sphingomyelin in the target membrane. The cholesterol dependence of fusion extent followed a sigmoidal curve, flattening at around 40 mol-%. This observation is consistent with earlier studies showing that cell infection of CHIKV is dependent on cholesterol (Bernard *et al*., 2010; Gay *et al*., 2012; Tsetsarkin *et al*., 2007; Tsetsarkin *et al*., 2011). Furthermore, our findings are in concordance with results obtained for SFV and SINV (Nieva *et al*., 1994; Smit *et al*., 1999). Cholesterol is known to influence the physical properties of membranes such as curvature, stability and fluidity and was found to promote insertion of the E1 fusion protein into the target membranes (Kielian & Helenius, 1984; Klimjack *et al.,* 1994; Mooney *et al*., 1975; Nieva *et al*., 1994; Smit

et al., 1999; Umashankar *et al*., 2008; Wahlberg *et al*., 1992). Our observation that cholesterol does not influence the kinetics of fusion suggests that it indeed functions as a binding cofactor rather than exerting its function by altering the physical properties of the target membrane, with no role in the rate-limiting steps leading to fusion.

No data on sphingomyelin dependency was available so far for CHIKV. We found that CHIKV fusion is strongly dependent on sphingomyelin in the target membrane. Relatively small amounts (6.6 mol-%) are sufficient for near-optimal fusion efficiency. In the absence of sphingomyelin, we observed residual fusion activity in the bulk assay (7±1%), and to a lesser extent (1±1%) also in the single-particle assay. Residual fusion activity at 37°C in the absence of sphingomyelin has been described for SFV (Chatterjee *et al*., 2002; Waarts *et al*., 2002), but not for SINV (Smit *et al*., 1999). It has been found that sphingolipids support cholesterol-mediated virus binding and stimulate the conformational changes required for membrane fusion (Ahn *et al*., 2002; Moesby *et al*., 1995; Nieva *et al*., 1994; Samsonov *et al*., 2002). In line with these findings, we observed that the fusion rate of CHIKV is not dependent on sphingomyelin concentrations, and therefore not dependent on the physical properties of the membrane that would vary with changing sphingomyelin concentrations.

Using the single-particle assay, we found that multiple rate-limiting steps precede CHIKV hemifusion. At pH 6.2, 6.0 and 4.7, we obtained hemifusion kinetic data for a large number of individual particles to be able to resolve the rise-and-decay behaviour in the distribution of hemifusion times. This is a characteristic of a process having multiple, equally fast rate-limiting steps. These steps could be sequential or parallel. For the range of proton concentrations (thirtyfold difference between pH 6.2 and 4.7) investigated, the number of steps was found to be in between 2 and 3. In the case of mechanistically distinct sequential steps that happen to have the same rate of progression, the one being proton-dependent would become the slowest, rate-limiting step at high pH, reducing the *N* to a value close to 1. In line with a similar reasoning previously used to rationalize single-particle fusion kinetics of influenza virus (Floyd *et al*., 2008), it seems more plausible from our data that there are several parallel steps required. In our opinion, it is likely that this feature reflects the requirement to have several copies of the fusion trimer to mediate fusion. Indeed, low-temperature electron micrograph experiments have shown the assembly of rings of fusion protein trimers on the outside of the virion (Gibbons *et al*., 2004b). The concerted action of assembled trimers then could give rise to the observed rise-and-decay hemifusion distributions. Alternatively, the formation of the fusogenic trimer from the individual E1 monomers could be rate limiting. We are currently working on obtaining an even more detailed molecular insight in the fusion process to test these hypotheses.

We report here the application of a bulk and single-particle fusion assay to study CHIKV hemifusion and show good consistency in results between these two approaches. The main advantage of the bulk assay lies in the fact that it possesses a high throughput and can therefore be used for a broad and detailed characterization of fusion. The single-particle approach enables kinetic information to be obtained at higher time resolution and devoid of dephasing effects as present in bulk assays. On the other hand, because of the technically challenging nature of the single-particle experiments, the single-particle experiments have a lower throughput and require more labour-intensive data analysis compared to the bulk assay. By using the combination of the two assays we arrive at an improved kinetic picture of CHIKV fusion, proving it a promising route for further research into the mechanistically guided search of fusion inhibitors. Further study of CHIKV fusion involving mutant virions and

fusion-inhibiting antibodies will be needed to further elucidate the molecular mechanisms involved in fusion.

Materials & Methods

Production, labelling and inactivation of viruses. CHIKV strain S27 (kindly provided by S. Günther, Bernhard-Nocht-Institute for Tropical Medicine), which was isolated in Tanzania in 1953 (Ross, 1956), was propagated in Vero-WHO cells to obtain seed stocks. The cells were maintained in DMEM (PAA laboratories) supplemented with 5% fetal bovine serum (FBS), 100 U/ml penicillin and 100 mg/ml streptomycin at 37 °C and with 5% CO_2. For virus production, a confluent monolayer of Vero-WHO cells was infected at an multiplicity of infection (MOI) of 0.01. At 48 hours post infection (hpi), the cell supernatant was harvested and cleared from cell debris by low-speed centrifugation, frozen in liquid nitrogen, and stored at -80 °C.

Virus for the bulk fusion assay was labelled biosynthetically with pyrene, essentially as described before for SFV and SINV (Smit *et al*., 1999; Waarts *et al*., 2002). Briefly, baby hamster kidney cells (BHK)-21 were cultured in the presence of 15 µg/ml of 1-pyrenehexadecanoic acid (Invitrogen) 48 hours prior to infection in RPMI (Life Technologies) supplemented with 10% FBS, 100 U/ml penicillin, and 100 mg/ml streptomycin at 37 °C and with 5% CO_2. BHK-21 cells were infected at MOI 4 and at 24 hpi, the cell supernatant was harvested and cleared from cell debris by low-speed centrifugation. Subsequently, the pyrene-labelled CHIKV particles were pelleted by ultracentrifugation in a Beckmann type 19 rotor at 54,000 × g for 2.5 hours. The virus was purified on a continuous sucrose (20/55% w/v) gradient by ultracentrifugation in a Beckmann SW 41 rotor overnight at 50,000 × g.

The virus preparations used for the single-particle fusion assay were generated and purified in the same fashion, except that the virus was propagated in the absence of pyrene. The purified CHIKV particles were subsequently labelled with the octadecyl rhodamine B chloride (R18; Invitrogen) fluorophore. For this purpose, 1×10^{11} to 2.2×10^{11} particles of purified and inactivated (see section *single-particle assay*) CHIKV were diluted in HNE (5 mM Hepes, 145 mM NaCl, 0.2 mM EDTA) and R18 dissolved in DMSO was added to a final concentration of 1µM. Subsequently, the virus solution was rotated at room temperature for 1 hour. A gel-filtration column (PD-10 desalting column; GE Healthcare) was used to separate the virus from unincorporated dye. The most concentrated fractions were combined and used undiluted in the experiment. To test whether labelling influences viral infectivity, active virus was labelled using the same methods for use in infectivity assays. At the timescale of our experiments, no R18 flip-flop occurred, which would be visible as a loss of virus particle intensity before the pH drop.

The number of physical particles was determined by a standard phosphate assay (Bottcher, 1961) using a value of 4.6×10^{-20} mol of phosphate per particle (Laine *et al*., 1973) and with quantitative PCR (qPCR). The qPCR was performed as described previously for Dengue virus (van der Schaar *et al*., 2007). Briefly, viral cDNA was synthesized by reverse transcriptase (RT) PCR using the forward primer 5'-AGCTCCGCGTCCTTTACCA-3' and the reverse primer 5'-GCCAAATTGTCCTGGTCTTCCT-3'. For the qPCR, the TaqMan probe 5'-FAM-CAC TGTAACTGCCTATGCAAACGGCGAC-TAMRA-3' was added. DNA was amplified for 40 cycles of 15 s at 95 °C and 60 s at 60 °C. Determination of the number of RNA copies was performed with a standard curve (correlation co-efficient > 0.995) of a quantified CHIKV plasmid containing the E1 sequences (pCHIKV-LS3 1B) constructed with standard DNA techniques. The infectivity of the virus was determined by a standard plaque assay on Vero-WHO cells. The specific infectivity was calculated by dividing the number of physical particles or genome-containing particles (GCP) by the number of PFU. As can be seen in Table S1, there is no significant difference between

the specific infectivity calculated with GCPs and the specific infectivity calculated with the physical particle concentration.

Preparation of liposomes and supported lipid bilayers. Liposomes (200 nm in diameter) were prepared by a freeze-thaw extrusion procedure as described before (Smit *et al*., 1999). Unless specified otherwise, liposomes consisted of phosphatidylcholine (PC) from egg yolk, phosphatidylethanolamine (PE) prepared from transphosphatidylation of egg PC, sphingomyelin (SPM) from porcine brain, and cholesterol from ovine wool in a molar ratio of 1:1:1:1.5. In experiments with lower SPM concentrations, SPM was replaced with an equal molar amount of PC to maintain the phospholipid-to-cholesterol ratio of 2:1. All lipids were purchased from Avanti Polar Lipids. Lipids and the phospholipid-to-cholesterol-ratio were chosen to approximate the lipid composition within the endosomal compartment (Kolter & Sandhoff, 2010; van Meer *et al*., 2008).

For the single-particle assay, liposomes (200 nm) were also prepared by freeze-thaw extrusion. Liposomes consisted of 1:1:1:1.5:2×10^{-5} ratio of 1,2-dioleoyl-*sn*-glycero-3-phosphocholine (DOPC), 1,2-dioleoyl-*sn*-glycero-3-phosphoethanolamine (DOPE), porcine brain sphingomyelin (SPM), ovine wool cholesterol and 1,2-dioleoyl-sn-glycero-3-phosphoethanolamine-N-(biotinyl) (Biotin-PE), unless otherwise specified.

Fusion assays

Throughout the report we will refer to (hemi)fusion as fusion, as the assays used do not distinguish content mixing from lipid mixing.

(i) Bulk fusion assay. Fusion of pyrene-labelled CHIKV with liposomes at 37°C was monitored in a Fluorolog 3-22 fluorometer (BFi Optilas, Alphen an den Rijn, The Netherlands), as described before (Smit *et al*., 1999; Thompson *et al*., 2009). Pyrene-labelled CHIKV (1,5 µM viral phospholipid, corresponds to 4×10^{10} virions) was mixed with an excess of liposomes (400 µM phospholipid, corresponding to 6×10^{10} liposomes) in a total of 665 µl in HNE buffer (5 mM HEPES, 150 mM NaCl, 0.1 mM EDTA) in a quartz cuvette. After 60 seconds of incubation with constant magnetic stirring, the pH was lowered by adding 35 µl of 0.1 M MES with 0.2 M acetic acid pretitrated with NaOH to achieve the desired pH. The fusion scale was calibrated such that 0% fusion corresponded to the initial excimer fluorescence value. 100% of fusion was set equal to the signal obtained by adding 35µl of 0.2 M octaethyleneglycol monododecyl ether ($C_{12}E_8$; Sigma-Aldrich) which caused an infinite dilution of the probe. The total fusion extent was determined by calculating the average signal between of 50 and 60 s after the pH drop. Curves were corrected for bleaching of the dye by subtracting the linearized control curve at pH 7.4.

To analyse whether CHIKV is inactivated by low pH in the absence of target membranes, the protocol was slightly adapted. In this case, HNE was mixed with 4×10^{10} virions and the pH was lowered to pH 5.0 with 0.1 M MES, 0.2 M acetic acid pre-titrated with NaOH. Pre-acidified liposomes were added to the measurement at the indicated time points to measure remaining fusion activity. For the back-neutralisation experiments, the virions were acidified as described above. After 90 seconds of acidification, the mixture was back-neutralised to pH 8.0 by a pre-titrated volume of NaOH. Then, liposomes in HNE (pH 7.4) were added and the mixture was re-acidified to pH 5.0 (t=0) and fusion was measured. Control experiments were performed with the same time intervals without pre-acidification and back-neutralisation.

(ii) Single-particle fusion assay. Use of the virus in our single-particle microscope outside a BSL-3 environment necessitated inactivation, which was achieved by UV

radiation using a 2 × 8 watt 254 nm UV lamp (VWR) until infectivity remained below 75 PFU/ml. The single-particle fusion assay showed that CHIKV is still fusogenic after treatment with UV radiation, with no significant change in fusion characteristics when compared to the bulk assay data.

Single-particle fusion experiments were performed using an assay we developed previously to visualize influenza fusion (Floyd *et al*., 2008), modified to perform all experiments at 37 °C. Glass microscope coverslips (24 × 50 mm, No. 1.5; VWR) were cleaned using 30 minute sonications in isopropanol and acetone, rinsing in between with deionized water, and finally 10 minutes in an oxygen plasma cleaner. Coverslips were stored in desiccated vacuum. Polydimethylsiloxane (PDMS) flow cells were prepared by pouring and hardening on a photolithography masks, essentially as before (Brandenburg *et al*., 2013).

A schematic overview of the setup is shown in Fig. 3(a)-(c). Imaging was performed on a home-built Total Internal Reflection Fluorescence (TIRF) microscope, using an inverted microscope (Olympus IX-71) and a high numerical aperture, oil-immersion objective (NA 1.45, 60x; Olympus). The flow cell was kept at elevated temperature in a heating block (Pecon GmbH), with the microscope objective thermally isolated from the microscope using a spacer ring (Bioptechs Inc.) and heated with a ring heater (Tokai Hit) to prevent local cooling of the flow cell. To provide pre-heated low pH buffer at short notice, a serpentine-shaped channel was included on the flow cell proximally to the channel of observation (see Fig. 3b), enabling acidification times of down to 0.5 s, necessary for the fast-fusing CHIKV. Liposomes were flushed into the flow cell and a planar lipid bilayer was allowed to form over the course of 20 minutes by the vesicle-spreading method (Nollert *et al*., 1995). Membrane fluidity was confirmed by Fast Recovery After Photobleaching (data not shown). Virions were docked non-specifically to the lipid bilayer (see Fig. 3c). Fluorescein-labelled streptavidin (Life Technologies) was introduced into the flow cell to bind to the membrane-incorporated Biotin-PE and serve its pH-dependent fluorescence as an optical readout of the exact moment of the pH decrease. The aqueous environment was acidified by flowing in citric acid buffer (10 mM, 140 mM NaCl) of calibrated pH at 300 µL/min for 8 s. The fluorophores were excited using 488 nm and 561 nm lasers (Coherent Inc.). Viral membrane fluorescence (red) and fluorescein pH drop fluorescence (green) were projected on different halves of an EM-CCD camera (Hamamatsu). Movies were acquired at 20 frames per second.

Analysis. Home-written software in MATLAB was used to extract the fluorescence signals corresponding to the pH drop signal and individual virions, essentially as described before (Floyd *et al*., 2008) (Fig. 3c). The fluorescein pH-drop signal was integrated over the entire field of view and the t=0 of the experiment defined as the point at which *Erfc*[1]/2 (~8%) intensity remained, with *Erfc*[] denoting the complementary error function. The lag time to hemifusion of n individual particles was then determined manually, binned per time unit and plotted in a histogram with $n^{1/2}$ bins. Next, we fitted a gamma distribution to the histogram to obtain the number of steps N and rate k of each step, the distribution resulting from N identical, rate-limiting steps (Floyd *et al*., 2010). To take into account the finite width of the pH drop at pH 4.7, the gamma distribution was convoluted in Mathematica with the known fluorescein signal derivative (a Gaussian function, see Fig. S2). For different values of N the rate k was then fitted.

Acknowledgements

We are grateful to S. Günther, Bernhard-Nocht-Institute for Tropical Medicine, Hamburg, Germany, for providing the chikungunya virus strain S27. We thank Jason Otterstrom, Mariana Ruiz Silva and Tabitha Hoornweg for technical assistance and helpful discussions. This work was supported by the Dutch Organization for Scientific research (NWO- Earth and Life Sciences (grant to JMS) and by the University Medical Center Groningen (grant to MKSvD-R). AMvO would like to acknowledge funding from the Dutch Organization for Scientific Research (NWO; *Vici* 680-47-607) and the European Research Council (ERC Starting 281098). JSB is supported by the Zernike Institute for Advanced Materials.

References

Ahn A., Gibbons D. L., Kielian M. (2002). The fusion peptide of semliki forest virus associates with sterol-rich membrane domains. *J Virol* **76**, 3267-3275.

Bernard E., Solignat M., Gay B., Chazal N., Higgs S., Devaux C., Briant L. (2010). Endocytosis of chikungunya virus into mammalian cells: Role of clathrin and early endosomal compartments. *PLoS One* **5**, e11479.

Bottcher C. S. F. (1961). A rapid and sensitive submicro phosphorus determination. *Ann Chim Acta* **24**, 203-204.

Brandenberg O. F., Magnus C., Rusert P., Regoes R. R., Trkola A. (2015). Different infectivity of HIV-1 strains is linked to number of envelope trimers required for entry. *PLoS Pathog* **11**, e1004595.

Brandenburg B., Koudstaal W., Goudsmit J., Klaren V., Tang C., Bujny M. V., Korse H. J., Kwaks T., Otterstrom J. J.& other authors. (2013). Mechanisms of hemagglutinin targeted influenza virus neutralization. *PLoS One* **8**, e80034.

Bron R., Wahlberg J. M., Garoff H., Wilschut J. (1993). Membrane fusion of semliki forest virus in a model system: Correlation between fusion kinetics and structural changes in the envelope glycoprotein. *EMBO J* **12**, 693-701.

Burt F. J., Rolph M. S., Rulli N. E., Mahalingam S., Heise M. T. (2012). Chikungunya: A re-emerging virus. *Lancet* **379**, 662-671.

Centers for Disease Control and Prevention (2015). Chikungunya in the Americas. http://www.cdc.gov/chikungunya/geo/americas.html. Accessed on February 3rd 2015.

Chatterjee P. K., Eng C. H., Kielian M. (2002). Novel mutations that control the sphingolipid and cholesterol dependence of the semliki forest virus fusion protein. *J Virol* **76**, 12712-12722.

Costello D. A., Lee D. W., Drewes J., Vasquez K. A., Kisler K., Wiesner U., Pollack L., Whittaker G. R., Daniel S. (2012). Influenza virus-membrane fusion triggered by proton uncaging for single particle studies of fusion kinetics. *Anal Chem* **84**, 8480-8489.

Danieli T., Pelletier S. L., Henis Y. I., White J. M. (1996). Membrane fusion mediated by the influenza virus hemagglutinin requires the concerted action of at least three hemagglutinin trimers. *J Cell Biol* **133**, 559-569.

Enserink M. (2014). Infectious diseases. crippling virus set to conquer western hemisphere. *Science* **344**, 678-679.

Enserink M. (2007). Infectious diseases. chikungunya: No longer a third world disease. *Science* **318**, 1860-1861.

Fischer M., Staples J. E., Arboviral Diseases Branch, National Center for Emerging and Zoonotic Infectious Diseases, CDC. (2014). Notes from the field: Chikungunya virus spreads in the americas - caribbean and south america, 2013-2014. *MMWR Morb Mortal Wkly Rep* **63**, 500-501.

Floyd D. L., Harrison S. C., van Oijen A. M. (2010). Analysis of kinetic intermediates in single-particle dwell-time distributions. *Biophys J* **99**, 360-366.

Floyd D. L., Ragains J. R., Skehel J. J., Harrison S. C., van Oijen A. M. (2008). Single-particle kinetics of influenza virus membrane fusion. *Proc Natl Acad Sci U S A* **105**, 15382-15387.

Gay B., Bernard E., Solignat M., Chazal N., Devaux C., Briant L. (2012). pH-dependent entry of chikungunya virus into aedes albopictus cells. *Infect Genet Evol* **12**, 1275-1281.

Gibbons D. L., Ahn A., Liao M., Hammar L., Cheng R. H., Kielian M. (2004a). Multistep regulation of membrane insertion of the fusion peptide of semliki forest virus. *J Virol* **78**, 3312-3318.

Gibbons D. L., Vaney M. C., Roussel A., Vigouroux A., Reilly B., Lepault J., Kielian M., Rey F. A. (2004b). Conformational change and protein-protein interactions of the fusion protein of semliki forest virus. *Nature* **427**, 320-325.

Glomb-Reinmund S. & Kielian M. (1998). The role of low pH and disulfide shuffling in the entry and fusion of semliki forest virus and sindbis virus. *Virology* **248**, 372-381.

Harrison S. C. (2008). Viral membrane fusion. *Nat Struct Mol Biol* **15**, 690-698.

Hinterdorfer P., Baber G., Tamm L. K. (1994). Reconstitution of membrane fusion sites. A total internal reflection fluorescence microscopy study of influenza hemagglutinin-mediated membrane fusion. *J Biol Chem* **269**, 20360-20368.

Hoekstra D., de Boer T., Klappe K., Wilschut J. (1984). Fluorescence method for measuring the kinetics of fusion between biological membranes. *Biochemistry* **23**, 5675-5681.

Imai M., Mizuno T., Kawasaki K. (2006). Membrane fusion by single influenza hemagglutinin trimers. kinetic evidence from image analysis of hemagglutinin-reconstituted vesicles. *J Biol Chem* **281**, 12729-12735.

Ivanovic T., Choi J. L., Whelan S. P., van Oijen A. M., Harrison S. C. (2013). Influenza-virus membrane fusion by cooperative fold-back of stochastically induced hemagglutinin intermediates. *Elife* **2**, e00333.

Kielian M., Chanel-Vos C., Liao M. (2010). Alphavirus entry and membrane fusion. *Viruses* **2**, 796-825.

Kielian M. C. & Helenius A. (1984). Role of cholesterol in fusion of semliki forest virus with membranes. *J Virol* **52**, 281-283.

Kielian M. (2014). Mechanisms of virus membrane fusion proteins. *Annual Review of Virology* **1**, 171-189.

Klimjack M. R., Jeffrey S., Kielian M. (1994). Membrane and protein interactions of a soluble form of the semliki forest virus fusion protein. *J Virol* **68**, 6940-6946.

Kolter T. & Sandhoff K. (2010). Lysosomal degradation of membrane lipids. *FEBS Lett* **584**, 1700-1712.

Kucharz E. J. & Cebula-Byrska I. (2012). Chikungunya fever. *Eur J Intern Med* **23**, 325-329.

Laine R., Soderlund H., Renkonen O. (1973). Chemical composition of semliki forest virus. *Intervirology* **1**, 110-118.

Lescar J., Roussel A., Wien M. W., Navaza J., Fuller S. D., Wengler G., Wengler G., Rey F. A. (2001). The fusion glycoprotein shell of semliki forest virus: An icosahedral assembly primed for fusogenic activation at endosomal pH. *Cell* **105**, 137-148.

Leung J. Y., Ng M. M., Chu J. J. (2011). Replication of alphaviruses: A review on the entry process of alphaviruses into cells. *Adv Virol* **2011**, 249640.

Li L., Jose J., Xiang Y., Kuhn R. J., Rossmann M. G. (2010). Structural changes of envelope proteins during alphavirus fusion. *Nature* **468**, 705-708.

Lu Y. E., Cassese T., Kielian M. (1999). The cholesterol requirement for sindbis virus entry and exit and characterization of a spike protein region involved in cholesterol dependence. *J Virol* **73**, 4272-4278.

Melikyan G. B., Barnard R. J., Abrahamyan L. G., Mothes W., Young J. A. (2005). Imaging individual retroviral fusion events: From hemifusion to pore formation and growth. *Proc Natl Acad Sci U S A* **102**, 8728-8733.

Moesby L., Corver J., Erukulla R. K., Bittman R., Wilschut J. (1995). Sphingolipids activate membrane fusion of semliki forest virus in a stereospecific manner. *Biochemistry* **34**, 10319-10324.

Mooney J. J., Dalrymple J. M., Alving C. R., Russell P. K. (1975). Interaction of sindbis virus with liposomal model membranes. *J Virol* **15**, 225-231.

Nieva J. L., Bron R., Corver J., Wilschut J. (1994). Membrane fusion of semliki forest virus requires sphingolipids in the target membrane. *EMBO J* **13**, 2797-2804.

Niles W. D. & Cohen F. S. (1991). Fusion of influenza virions with a planar lipid membrane detected by video fluorescence microscopy. *J Gen Physiol* **97**, 1101-1119.

Nollert P., Kiefer H., Jahnig F. (1995). Lipid vesicle adsorption versus formation of planar bilayers on solid surfaces. *Biophys J* **69**, 1447-1455.

Pal R., Barenholz Y., Wagner R. R. (1988). Pyrene phospholipid as a biological fluorescent probe for studying fusion of virus membrane with liposomes. *Biochemistry* **27**, 30-36.

Powers A. M., Brault A. C., Shirako Y., Strauss E. G., Kang W., Strauss J. H., Weaver S. C. (2001). Evolutionary relationships and systematics of the alphaviruses. *J Virol* **75**, 10118-10131.

Ross R. W. (1956). A laboratory technique for studying the insect transmission of animal viruses, employing a bat-wing membrane, demonstrated with two african viruses. *J Hyg (Lond)* **54**, 192-200.

Samsonov A. V., Chatterjee P. K., Razinkov V. I., Eng C. H., Kielian M., Cohen F. S. (2002). Effects of membrane potential and sphingolipid structures on fusion of semliki forest virus. *J Virol* **76**, 12691-12702.

Sanchez-San Martin C., Sosa H., Kielian M. (2008). A stable prefusion intermediate of the alphavirus fusion protein reveals critical features of class II membrane fusion. *Cell Host Microbe* **4**, 600-608.

Sanchez-San Martin C., Nanda S., Zheng Y., Fields W., Kielian M. (2013). Cross-inhibition of chikungunya virus fusion and infection by alphavirus E1 domain III proteins. *J Virol* **87**, 7680-7687.

Schwartz O. & Albert M. L. (2010). Biology and pathogenesis of chikungunya virus. *Nat Rev Microbiol* **8**, 491-500.

Smit J. M., Bittman R., Wilschut J. (1999). Low-pH-dependent fusion of sindbis virus with receptor-free cholesterol- and sphingolipid-containing liposomes. *J Virol* **73**, 8476-8484.

Sourisseau M., Schilte C., Casartelli N., Trouillet C., Guivel-Benhassine F., Rudnicka D., Sol-Foulon N., Le Roux K., Prevost M. C.& other authors. (2007). Characterization of reemerging chikungunya virus. *PLoS Pathog* **3**, e89.

Strauss J. H. & Strauss E. G. (1994). The alphaviruses: Gene expression, replication, and evolution. *Microbiol Rev* **58**, 491-562.

Thiberville S. D., Moyen N., Dupuis-Maguiraga L., Nougairede A., Gould E. A., Roques P., de Lamballerie X. (2013). Chikungunya fever: Epidemiology, clinical syndrome, pathogenesis and therapy. *Antiviral Res* **99**, 345-370.

Thompson B. S., Moesker B., Smit J. M., Wilschut J., Diamond M. S., Fremont D. H. (2009). A therapeutic antibody against west nile virus neutralizes infection by blocking fusion within endosomes. *PLoS Pathog* **5**, e1000453.

Tomasello D. & Schlagenhauf P. (2013). Chikungunya and dengue autochthonous cases in europe, 2007-2012. *Travel Med Infect Dis* **11**, 274-284.

Tsetsarkin K. A., McGee C. E., Higgs S. (2011). Chikungunya virus adaptation to aedes albopictus mosquitoes does not correlate with acquisition of cholesterol dependence or decreased pH threshold for fusion reaction. *Virol J* **8**, 376-422X-8-376.

Tsetsarkin K. A., Vanlandingham D. L., McGee C. E., Higgs S. (2007). A single mutation in chikungunya virus affects vector specificity and epidemic potential. *PLoS Pathog* **3**, e201.

Umashankar M., Sanchez-San Martin C., Liao M., Reilly B., Guo A., Taylor G., Kielian M. (2008). Differential cholesterol binding by class II fusion proteins determines membrane fusion properties. *J Virol* **82**, 9245-9253.

van der Schaar H. M., Rust M. J., Waarts B. L., van der Ende-Metselaar H., Kuhn R. J., Wilschut J., Zhuang X., Smit J. M. (2007). Characterization of the early events in dengue virus cell entry by biochemical assays and single-virus tracking. *J Virol* **81**, 12019-12028.

van Meer G., Voelker D. R., Feigenson G. W. (2008). Membrane lipids: Where they are and how they behave. *Nat Rev Mol Cell Biol* **9**, 112-124.

Vancini R., Wang G., Ferreira D., Hernandez R., Brown D. T. (2013). Alphavirus genome delivery occurs directly at the plasma membrane in a time- and temperature-dependent process. *J Virol* **87**, 4352-4359.

Voss J. E., Vaney M. C., Duquerroy S., Vonrhein C., Girard-Blanc C., Crublet E., Thompson A., Bricogne G., Rey F. A. (2010). Glycoprotein organization of chikungunya virus particles revealed by X-ray crystallography. *Nature* **468**, 709-712.

Waarts B. L., Bittman R., Wilschut J. (2002). Sphingolipid and cholesterol dependence of alphavirus membrane fusion. lack of correlation with lipid raft formation in target liposomes. *J Biol Chem* **277**, 38141-38147.

Waarts B. L., Smit J. M., Aneke O. J., McInerney G. M., Liljestrom P., Bittman R., Wilschut J. (2005). Reversible acid-induced inactivation of the membrane fusion protein of semliki forest virus. *J Virol* **79**, 7942-7948.

Wahlberg J. M. & Garoff H. (1992). Membrane fusion process of semliki forest virus. I: Low pH-induced rearrangement in spike protein quaternary structure precedes virus penetration into cells. *J Cell Biol* **116**, 339-348.

Wahlberg J. M., Boere W. A., Garoff H. (1989). The heterodimeric association between the membrane proteins of semliki forest virus changes its sensitivity to low pH during virus maturation. *J Virol* **63**, 4991-4997.

Wahlberg J. M., Bron R., Wilschut J., Garoff H. (1992). Membrane fusion of semliki forest virus involves homotrimers of the fusion protein. *J Virol* **66**, 7309-7318.

Wengler G., Koschinski A., Wengler G., Repp H. (2004). During entry of alphaviruses, the E1 glycoprotein molecules probably form two separate populations that generate either a fusion pore or ion-permeable pores. *J Gen Virol* **85**, 1695-1701.

Wessels L., Elting M. W., Scimeca D., Weninger K. (2007). Rapid membrane fusion of individual virus particles with supported lipid bilayers. *Biophys J* **93**, 526-538.

White J. & Helenius A. (1980). pH-dependent fusion between the semliki forest virus membrane and liposomes. *Proc Natl Acad Sci U S A* **77**, 3273-3277.

Figures

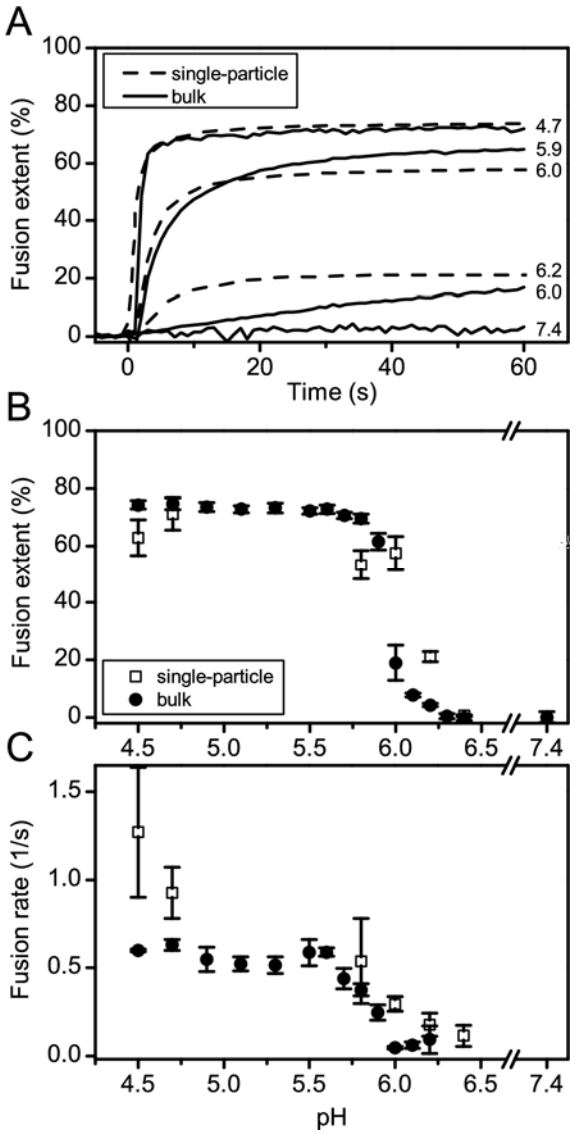

Fig. 1. Fusion of fluorescently labeled CHIKV with target membranes at low pH. (A) Representative fusion curves obtained with bulk (solid line) and single-particle (dashed line) assays. The pH value is shown next to the curve. (B) pH dependency of the extent of fusion. (C) Fusion rate (see text for definition, and table S2 for data values) of CHIKV as a function of pH. (B & C) Solid dots, bulk fusion assay; open squares, single-particle assay. For each condition, at least three independent experiments were performed for the bulk assay and 360-1316 particles were studied per condition in the single-particle assay. Error bars show standard error of the mean (SEM).

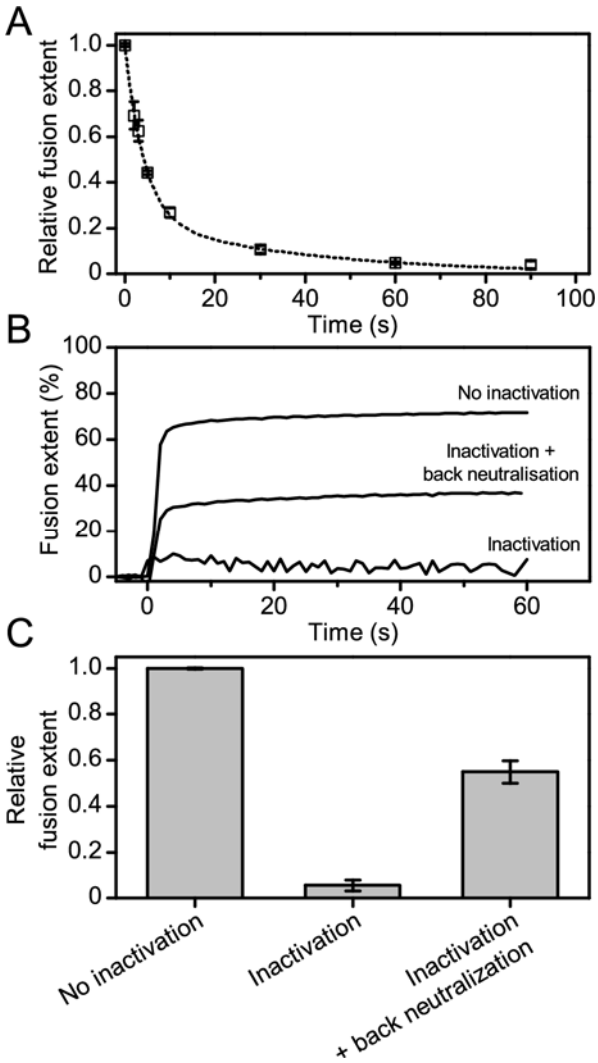

Fig. 2. Reversible inactivation of CHIKV due to low pH exposure in the absence of liposomes. Data points show mean±SEM for at least three independent experiments. (A) CHIKV virions were incubated at pH 5.0 prior to the addition of pre-acidified liposomes for the indicated time period. The extent of fusion is compared to an untreated control. Dashed line shows a double-exponential fit, indicating the presence of two populations. The first population comprises a fraction of 0.76±0.05 with time scale τ = 4.2±0.4 s-1, the second, a fraction of 0.24±0.05 and τ = 38±5 s-1. (B) Reversibility of low pH inactivation. Representative fusion curves of each condition are shown. The exact experimental protocol is described in the Material & Methods section. (C) Comparison of the fusion extents relative to the untreated control of the experiments of 90-seconds-inactivation (5±3%) and back-neutralisation (55±4%).

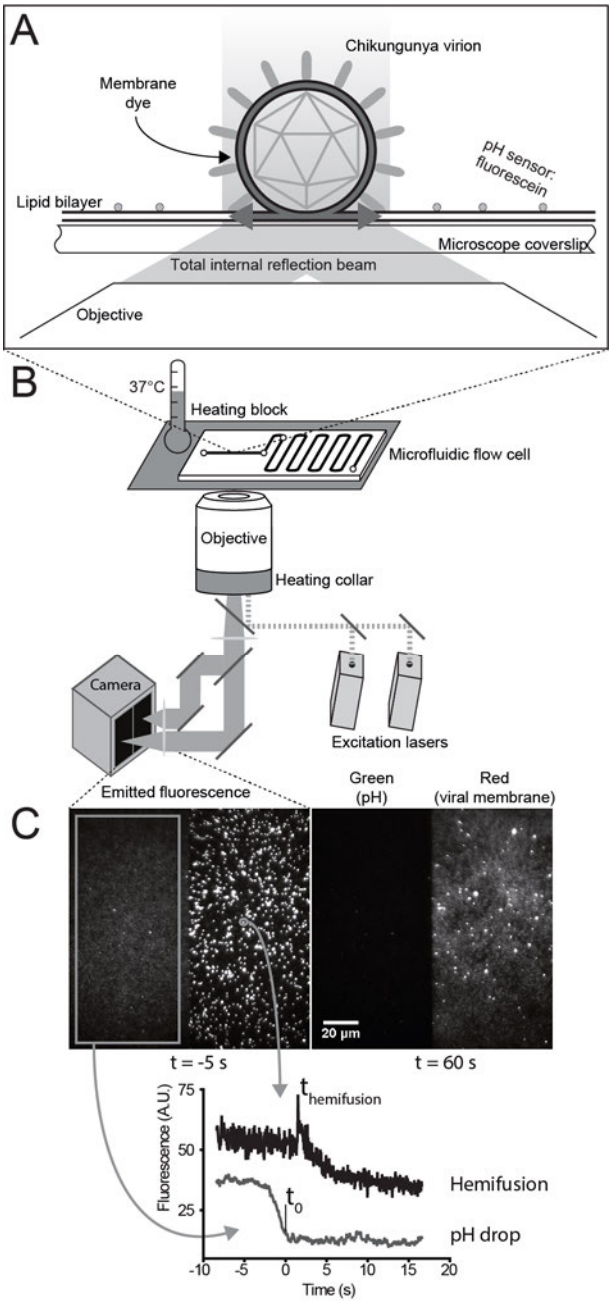

Fig. 3. Experimental design of the single-particle assay. (A) Virions labeled with a membrane dye (R18) bind to a glass-supported lipid bilayer. Hemifusion is induced by lowering the pH and observed with total internal reflection (TIRF) microscopy as the dequenching of R18 caused by its dissipation into the target membrane. Fluorescein molecules bound to the supported bilayer provide a readout of local pH conditions. (B) The microfluidic flow cell and microscope objective are kept at 37°C. Low pH buffer is incubated proximally to the channel of observation (left half of chip) in a serpentine-shaped flow channel (right half of chip) to provide constant-temperature and short acidification times. Emitted fluorescence is separated by color and collected onto different halves of an EM-CCD camera. (C) Pre- and post-acidification movie frames (top) and an example of the fluorescence time trajectories (bottom). The fluorescein signal defines the t=0 of the experiment and individual virus hemifusion lag times are identified. See also movie S1.

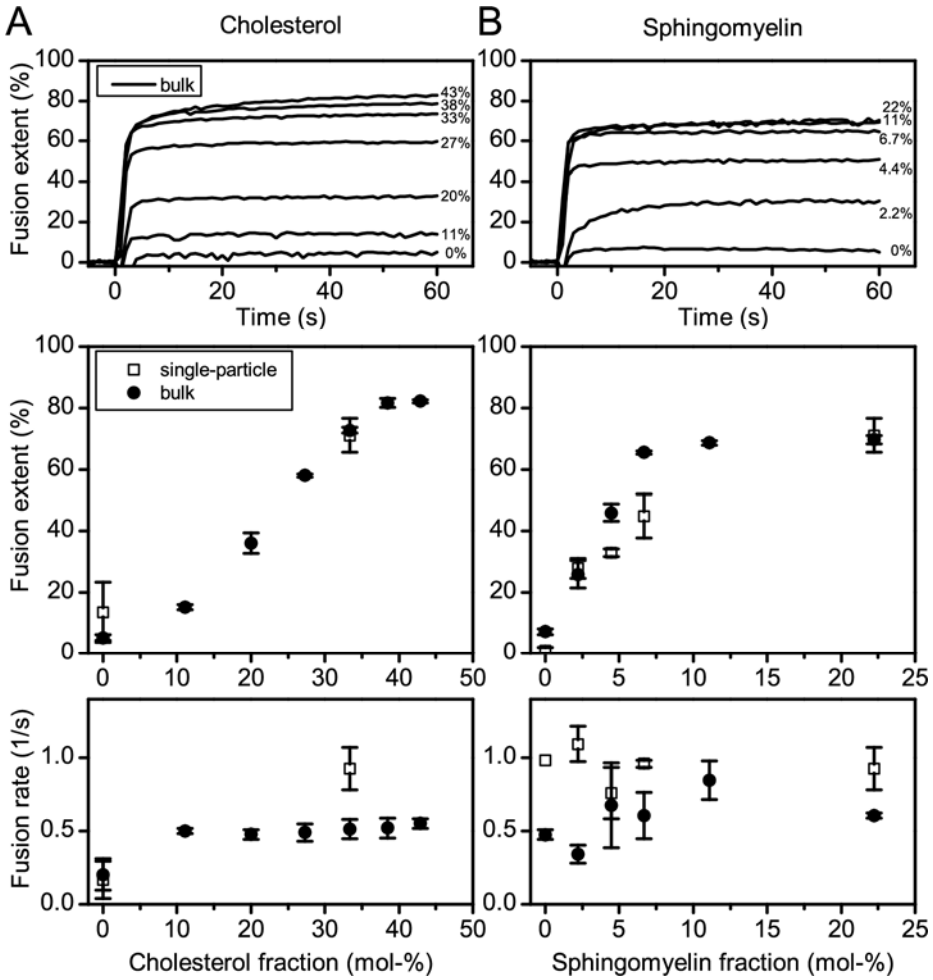

Fig. 4. Fusion of fluorescently labeled CHIKV with target membranes containing varying amounts of cholesterol and sphingomyelin. (A, top panel) Representative bulk fusion curves as a function of target-membrane cholesterol content. Target membrane cholesterol content is shown next to curves in mol-%. (A, middle panel) Extent of fusion quantified at varying cholesterol concentrations. Solid dots, bulk assay; open squares, single-particle assay. (A, bottom panel) Fusion rate at varying cholesterol concentrations. (B) Panels as by A, representing fusion characteristics as a function of target membrane sphingomyelin content. Target membrane sphingomyelin content is shown next to curves in mol-%.. For each condition, at least three independent experiments were performed for the bulk assay and 308-767 particles were studied per condition in the single-particle assay. Error bars show SEM.

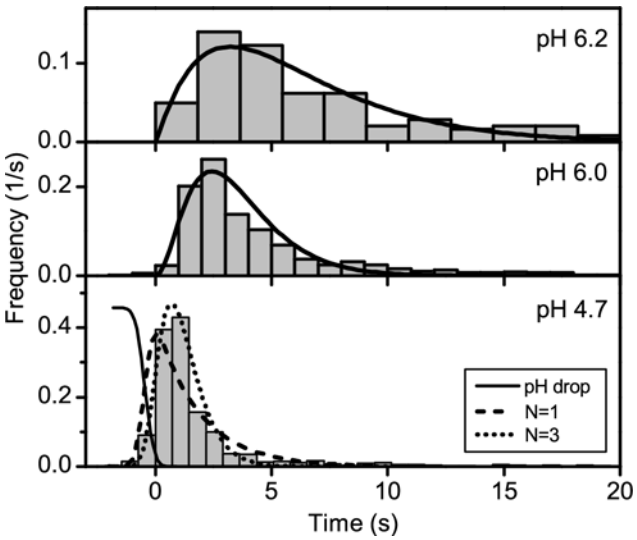

Fig. 5. Fusion lag time distributions of CHIKV at pH 6.2, 6.0 and 4.7. Elapsed time of individual virions between acidification and hemifusion for pH 6.2, 6.0 and 4.7 (n = 148, 605, 977 fusing virions respectively). The rise and decay indicates that several intermediate states precede the hemifusion event. For pH 6.2 and 6.0, fitted Gamma distributions (solid line; see text) are shown, with N = 2.1±0.4, 3.2±0.4 and k = 0.34±0.08 s-1, 0.9±0.2 s-1 respectively. For pH 4.7, the fits were modified to include the finite length of the pH drop (solid line; see text) and such fits with fixed N = 1 (dashed line; fitted k = 0.53±0.09 s-1) and N = 3 (dotted line; k = 1.22±0.06) are shown.